

Hard X-ray emission from elliptical galaxies

S.W. Allen¹, T. Di Matteo^{2*} and A.C. Fabian¹

1. Institute of Astronomy, Madingley Road, Cambridge CB3 0HA

2. Harvard-Smithsonian Center for Astrophysics, 60 Garden Street, Cambridge MA 02138, USA

ABSTRACT

We report the detection of hard X-ray emission components in the spectra of six nearby, giant elliptical galaxies observed with the ASCA satellite. The systems studied, which exhibit strong dynamical evidence for supermassive black holes in their nuclei, are M87, NGC 1399 and NGC 4696 (the dominant galaxies of the Virgo, Fornax and Centaurus clusters, respectively) and NGC 4472, 4636 and 4649 (three further giant ellipticals in the Virgo cluster). The ASCA data for all six sources provide clear evidence for hard emission components, which can be parameterized by power-law models with photon indices in the range $\Gamma = 0.6 - 1.5$ (mean value 1.2) and intrinsic $1 - 10$ keV luminosities of $2 \times 10^{40} - 2 \times 10^{42}$ erg s⁻¹. Our results imply the identification of a new class of accreting X-ray source, with X-ray spectra significantly harder than those of binary X-ray sources, Seyfert nuclei or low luminosity AGN, and bolometric luminosities relatively dominated by their X-ray emission. We discuss various possible origins for the hard X-ray emission and argue that it is most likely to be due to accretion onto the central supermassive black holes, via low-radiative efficiency accretion coupled with strong outflows. In the case of M87, our detected power-law flux is in good agreement with a previously-reported measurement from ROSAT High Resolution Imager observations, which were able to resolve the jet from the nuclear X-ray emission components. We confirm previous results showing that the use of multiphase models in the analysis of the ASCA data leads to determinations of approximately solar emission-weighted metallicities for the X-ray gas in the galaxies. We also present results on the individual element abundances in NGC 4636.

Key words: accretion, accretion disks – galaxies: abundances – galaxies:active – galaxies:nuclei – X-rays: galaxies – X-rays: ISM

1 INTRODUCTION

Observations of nearby galaxies provide convincing evidence for the existence of supermassive black holes. Although most such galaxies exhibit little or no nuclear activity, dynamical arguments based on the observed stellar and gas distributions firmly imply the presence of supermassive compact objects in their cores (*e.g.* Kormendy & Richstone 1995, Magorrian *et al.* 1998, Ho 1998, van der Marel 1999). Interestingly, these studies show that virtually all early-type galaxies host black holes with masses in the range $10^8 -$ a few 10^9 M_{\odot} . In disk galaxies, however, the (rather sparser) observations indicate that the black hole masses are typically of order 10^7 M_{\odot} (*e.g.* SgrA* in our own Galaxy, M31, and the maser galaxy NGC 4258), consistent with the black hole masses in galaxies being roughly proportional to the masses of the spheroidal components.

Although the central black hole masses in early type galaxies are large enough to be the remnants of

QSO phenomena (with luminosities ranging from 10^{46} to 10^{48} erg s⁻¹) and giant ellipticals are known to host radio galaxies and radio-loud quasars at high redshifts, in nearby ellipticals, only low-luminosity radio cores are commonly observed (Sadler, Jenkins & Kotanji 1989; Wrobel & Heershen 1991). Spiral galaxies, in contrast, frequently exhibit nuclear activity (*e.g.* Seyfert nuclei), with optical/UV emission, strong, power-law X-ray continua (with a typical intrinsic photon index, $\Gamma \sim 2$) and complex variability observed. Such phenomena are usually attributed to standard, thin-disk accretion, coupled with a hot coronal plasma with high radiative efficiencies.

Postulating that the early-type systems are simply ‘starved’ of fuel to power their activity appears implausible since these galaxies possess extensive hot, gaseous halos which will inevitably accrete onto their central black holes at rates which may be estimated using the Bondi (1952) formula (a lower limit). This accretion should give rise to far more activity than is observed, if the radiative efficiency is ~ 10 per cent, as is postulated in standard accretion theory (*e.g.* Fabian & Canizares 1988). All nearby elliptical

* Chandra Fellow

galaxies should then host active nuclei with luminosities exceeding $10^{45} \text{ erg s}^{-1}$. However, the available data show that the total X-ray luminosities of these galaxies rarely exceed $10^{42} \text{ erg s}^{-1}$, with only a small fraction of this flux being due to a central point source.

Accretion with such high radiative efficiency need not be universal, however. As suggested by several authors (Rees *et al.* 1982; Begelman, Blandford & Rees 1984; Fabian & Rees 1995) and successfully applied to a number of giant ellipticals in the Virgo cluster (Reynolds *et al.* 1996; Di Matteo & Fabian 1997a; Mahadevan 1997; Di Matteo *et al.* 1999a), the final stages of accretion in elliptical galaxies may occur via an advection-dominated accretion flow (ADAF; Narayan & Yi 1995; Abramowicz *et al.* 1995) at roughly the Bondi rates. Within the context of such an accretion mode, the quiescence of the nuclei in these systems is not surprising; when the accretion rate is low, the radiative efficiency of the accreting (low density) material will also be low. Other factors may also contribute to the low luminosities observed. As discussed by Blandford & Begelman (1999; and emphasized observationally by Di Matteo *et al.* 1999a), winds may transport energy, angular momentum and mass out of the accretion flows, resulting in only a small fraction of the material supplied at large radii actually accreting onto the central black holes.

If the accretion from the hot interstellar medium in elliptical galaxies (which should have relatively low angular momentum) proceeds directly into the hot, advection-dominated regime, and low-efficiency accretion is coupled with outflows (Di Matteo *et al.* 1999a), the question arises of whether *any* of the material entering into the accretion flows at large radii actually reaches the central black holes. The present observational data generally provide little or no evidence for detectable optical, UV or X-ray emission associated with the nuclear regions of these galaxies.

In this paper we present a detailed, multiphase analysis of high-quality ASCA X-ray spectra for six nearby elliptical galaxies; three central cluster galaxies and three giant ellipticals in the Virgo Cluster. We obtain clear detections of hard (mean-weighted photon index, $\Gamma = 1.2$) power-law, emission components in the integrated X-ray spectra of all six galaxies. Although our data do not allow us to unambiguously identify these components with the nuclear regions of the galaxies, we show that this emission is likely to be related to the accretion process and the presence of the central, supermassive black holes, which also power radio activity in the galaxies at varying levels.

The presence of hard X-ray emission components in the ASCA spectra of elliptical galaxies has previously been reported by a number of authors (*e.g.* Matsushita *et al.* 1994; Matsumoto *et al.* 1997; Buote & Fabian 1998). In general, however, these studies have associated the observed, hard components with a population of binary X-ray sources, the spectra of which can be approximated by bremsstrahlung models with typical temperatures of 4 – 7 keV (*e.g.* Fabiano, Trinchieri & Van Speybroeck 1987; White, Stella & Parmar 1988; Makishima *et al.* 1989; Tanaka *et al.* 1996; Christian & Swank 1998). The spectra of the hard X-ray emission components detected in the present sample of elliptical galaxies are significantly harder than those of binary X-ray sources or typical AGN, identifying these objects as, potentially, a new class of accreting source. (The ‘canonical’

photon index for AGN has $\Gamma \sim 1.8 - 2$; Nandra *et al.* 1997, Reynolds 1997; recent ASCA studies of low-luminosity AGN indicate photon indices in the range $\Gamma \sim 1.6 - 1.8$; *e.g.* M81; Ishiaki *et al.* 1996, Turner *et al.* 1996 or NGC 4258; Makishima *et al.* 1994) The X-ray luminosities of the present systems ($L_{X,1-10} = 2 \times 10^{40} - 2 \times 10^{42} \text{ erg s}^{-1}$) are similar to those of low luminosity AGN (*e.g.* Ho, Filippenko & Sargent 1997), although the large ($\sim 10^9 M_{\odot}$) black hole masses in their nuclei identifies them as far more inefficient radiators. The spectral energy distributions for the galaxies in our sample indicate that a significant fraction of their luminosities are emitted at X-ray wavelengths, with relatively low levels of optical and UV emission, which are dominant in typical AGN. These data, coupled with the presence of compact (possibly thermal synchrotron) radio cores, suggest a possible, ubiquitous presence of low-level nuclear activity in the nearby universe and provide important new constraints on the dominant accretion mechanisms in elliptical galaxy cores.

2 OBSERVATIONS AND DATA REDUCTION

2.1 Target selection

The targets selected for investigation are six well-studied, nearby elliptical galaxies, with high-quality ASCA observations available in public archives. The objects include three dominant cluster galaxies; the well known, low-luminosity radio galaxy M87 (NGC 4486) at the centre of the Virgo Cluster; NGC 1399, the giant elliptical at the centre of the Fornax Cluster and NGC 4696, the dominant galaxy of the Centaurus Cluster. These three galaxies, and especially M87, are key examples of quiescent active nuclei, containing nuclear black hole masses of $3 - 5 \times 10^9 M_{\odot}$ (Ford *et al.* 1995; Harms *et al.* 1994; Macchetto *et al.* 1998; Magorrian *et al.* 1998; although no direct mass measurement for NGC 4696 has been made) and exhibiting low-luminosity relativistic jets and FR-I-type radio emission. However, the luminosities of their nuclei are approximately three orders of magnitude less than would be expected if they were accreting at close to their Bondi rates, with a standard radiative efficiency (*e.g.* Reynolds *et al.* 1996).

The sample also includes three other giant ellipticals in the Virgo cluster; NGC 4649, 4472 and 4636. These galaxies contain almost completely inactive black holes, with measured masses ranging from a few $10^8 M_{\odot}$ to a few $10^9 M_{\odot}$ (Magorrian *et al.* 1998) and predicted X-ray luminosities (if the accretion occurs at the Bondi rate with a standard radiative efficiency) four to five orders of magnitude greater than is observed (Di Matteo *et al.* 1999a).

The central cluster galaxies provide an extreme illustration of the phenomenon of quiescent black holes. Beside possessing FR-I-type radio sources and very large black hole masses, these galaxies exist in extremely gas-rich environments *i.e.* in cooling flows at the centres of clusters, and are therefore ideal sources in which to study the physics of low-radiative efficiency accretion. However, these same reasons also imply that these galaxies are by no means typical. Despite exhibiting lower luminosities, the properties of the other three ellipticals in our sample, which do not exist in such preferential locations, may be more easily generalized

Table 1. Summary of the ASCA Observations

Cluster	D_L	Date	S0	S1	G2	G3
M87	18.0	1993 Jun 07	13633	14668	16874	16874
NGC 1399(1)	29.0	1993 Jul 15	16636	17678	19646	19646
NGC 1399(2)	—	1993 Jul 16	14266	16961	19741	19785
NGC 4696	62.6	1995 May 19	—	67650	70981	—
NGC 4472(1)	18.0	1993 Jun 30	17022	18314	22242	22240
NGC 4472(2)	—	1993 Jul 04	16461	18781	22739	22731
NGC 4636	18.0	1995 Dec 28	244180	245450	183290	183280
NGC 4649(1)	18.0	1994 Jan 07	21438	10669	40928	40926
NGC 4649(2)	18.0	1994 Jan 07	13775	—	—	—

Notes: Column 2 lists the luminosity distances (D_L) to the galaxies in Mpc. For the Virgo Cluster galaxies we assume a fixed distance of 18Mpc. For NGC 1399 and 4696 the distances are calculated using the optically-determined redshifts and an assumed cosmology of $H_0=50 \text{ km s}^{-1} \text{ Mpc}^{-1}$, $\Omega = 1$ and $\Lambda = 0$. Column 3 lists the dates of the observations. Columns 4–7 summarize the net exposure times (in seconds) in the four ASCA detectors, after all screening and cleaning procedures were carried out. For NGC 4696 only data from the S1 and G2 detectors were included in the analysis, due to residual calibration errors in the data from the other detectors for that observation. For NGC 1399, 4472 and 4649, the observations were made in two parts. For the second NGC 4649 observation, only the S0 data were of sufficient quality to be of use in the analysis.

to other systems. These three galaxies have also been studied at high radio frequencies and sub-mm wavelengths (Di Matteo *et al.* 1999a) and, when coupled with the reduced jet-radio-activity in these systems (and the ASCA data presented in this paper), provide further crucial constraints on the primary accretion mechanisms in the nuclei of elliptical galaxies.

2.2 The ASCA Observations and data reduction

The ASCA (Tanaka, Inoue & Holt 1994) observations were made over a two-and-a-half year period between 1993 June and 1995 December. The ASCA X-ray telescope array (XRT) consists of four nested-foil telescopes, each focussed onto one of four detectors; two X-ray CCD cameras, the Solid-state Imaging Spectrometers (SIS; S0 and S1) and two Gas scintillation Imaging Spectrometers (GIS; G2 and G3). The XRT provides a spatial resolution of ~ 3 arcmin (Half Power Diameter) in the energy range 0.5 – 10 keV. The SIS detectors provide excellent spectral resolution [$\Delta E/E = 0.02(E/5.9\text{keV})^{-0.5}$] over a 22×22 arcmin² field of view. The GIS detectors provide poorer energy resolution [$\Delta E/E = 0.08(E/5.9\text{keV})^{-0.5}$] but cover a larger circular field of view of ~ 50 arcmin diameter.

For our analysis of the ASCA data we have used the screened event lists from the rev2 processing of the data sets available on the Goddard-Space Flight Center (GSFC) ASCA archive (for details see the ASCA Data Reduction Guide, published by GSFC.) The data were reduced using the FTOOLS software (version 4.1) from within the XSELEKT environment (version 1.4). Further data-cleaning procedures as recommended in the ASCA Data Reduction Guide, including appropriate grade selection, gain corrections and manual screening based on the individual instrument light curves, were followed. A full summary of the observations is given in Table 1.

Spectra were extracted from all four ASCA detectors,

except for NGC 4696 for which the S0 and G3 data exhibited residual calibration errors and so were excluded from the analysis. The spectra were extracted from circular regions, centred on the peaks of the X-ray emission from the galaxies. For the SIS data, the radii of the regions studied were selected to minimize the number of chip boundaries crossed (thereby minimizing the systematic uncertainties introduced by such crossings) whilst covering as large a region of the galaxies as possible. Data from the regions between the chips were masked out and excluded. The final extraction radii for the SIS data are summarized in Table 2. Also noted are the chip modes used for the observations and the number of chips from which the extracted data were drawn. For the GIS data, a fixed extraction radius of 6 arcmin was adopted.

Background subtraction was carried out using the ‘blank sky’ observations of high Galactic latitude fields compiled during the performance verification stage of the ASCA mission. The background spectra were screened and grade selected in the same manner as the target observations and extracted from the same regions of the detectors. For the systems observed in 4-CCD mode, additional SIS background spectra were extracted from regions of the chips free from significant source counts (we note that this was not possible for the M87 observation due to the extended cluster emission which covers the full area of the detectors). The use of these on-chip backgrounds in place of the blank-sky backgrounds did not significantly alter the results.

For the SIS data, response matrices were generated using the FTOOLS SISRMG software (version 1.1). Where the extracted spectra covered more than a single chip, individual response matrices were created for each chip, which were then combined to form a counts-weighted mean matrix. For the GIS analysis, the response matrices issued by GSFC on 1995 March 6 were used.

Table 2. Extraction radii and chip modes for the SIS observations

Cluster	S0 (amin/kpc)	S1 (amin/kpc)	Chip Mode
M87	4.9/25.5	4.1/21.3	4(2)
NGC 1399(1)	4.2/35.1	3.7/30.9	4(1)
NGC 1399(2)	4.3/35.9	4.2/35.1	4(1)
NGC 4696	—	3.7/66.0	1(1)
NGC 4472(1)	3.7/19.3	3.7/19.3	4(1)
NGC 4472(2)	3.2/16.7	3.4/17.7	4(1)
NGC 4636	4.4/22.9	3.6/18.7	1(1)
NGC 4649(1)	3.8/19.8	2.9/15.1	4(2)
NGC 4649(2)	3.8/19.8	—	2(2)

The radii of the circular extraction regions for the SIS spectra (in arcmin and kpc) and the chip modes used in the observations (either 1, 2 or 4-CCD mode). The numbers in parentheses indicate the number of chips contributing to the extracted spectra. For the GIS data, a fixed extraction radius of 6 arcmin was used.

3 THE ANALYSIS OF THE ASCA DATA

3.1 The spectral models

The modeling of the X-ray spectra has been carried out using the XSPEC spectral fitting package (version 10.0; Arnaud 1996). For the SIS data, only counts in pulse height analyser (PHA) channels corresponding to energies between 0.6 and 10.0 keV were included in the analysis (the energy range over which the calibration of the SIS instruments is best-understood). For the GIS data, only counts in the energy range 1.0 – 10.0 keV were used. The spectra were grouped before fitting to ensure that χ^2 statistics could be reliably used (after background subtraction).

The spectra have been modeled using the plasma codes of Kaastra & Mewe (1993; incorporating the Fe L calculations of Liedahl, Osterheld & Goldstein 1995) and the photoelectric absorption models of Balucinska-Church & McCammon (1992). The data from all four detectors were included in the analysis, with the fit parameters linked to take the same values across the data sets. The exceptions to this were the emission measures of the (hot) plasma components, which model the extended X-ray halos of the galaxies and which, due to the different extraction radii used for the different detectors, were maintained as independent fit parameters.

The spectra were examined with a series of spectral models. (We have adopted the naming convention of Allen *et al.* 1999 from their analysis of nearby cluster spectra). The first model, Model B, consists of an isothermal plasma of temperature, kT , and metallicity, Z , in collisional equilibrium, at the optically-determined redshift for the galaxy, and absorbed by a column density N_H . Metallicities are measured relative to solar photospheric values of Anders & Grevesse (1989) with the various elements assumed to be present in their solar ratios. The second model, model D, included an additional, cooler plasma component of temperature, kT_2 , the normalization of which was a further free parameter in the fits. (This cooler component, where present,

is typically associated with the presence of a cooling flow in a cluster or galaxy). The metallicity of the cooler component was linked to that of the hotter gas. The cooler component was also assumed to be absorbed by an intrinsic column density, ΔN_H , of cold gas, which was a further free parameter in the fits. The abundances of metals in the absorbing gas were fixed at their solar values (Anders & Grevesse 1989).

Where it provided a significant statistical improvement, a third spectral model, model F, was also examined which was similar to model D but with the abundances of various individual elements also included as free parameters in the fits. This model was statistically preferred over model D for M87, NGC 4696 and NGC 4636.

Finally, a fourth spectral model, Model G, was investigated in which a power-law emission component was introduced into the previous best-fitting two-temperature plasma model (either model D or F, respectively). The power-law emission component was assumed to be absorbed by the same intrinsic column density acting on the cooler plasma emission component (since both components are expected to arise primarily from the central regions of the galaxies and/or clusters).

3.2 The requirement for multi-phase models and the metallicity of the X-ray gas

The results from the spectral modeling are summarized in Table 3. We see that the two-temperature model, model D, invariably provides a much better description of the ASCA spectra for the galaxies than the single-temperature model (model B), with a typical reduction in χ^2 of a few hundred for the introduction of only three additional degrees of freedom in the fit. For NGC 1399, 4472 and 4649, the use of the two temperature model results in a significant increase in the inferred metallicity of the X-ray gas in the galaxies, from values of 0.2 – 0.4 solar with spectral model B, to values consistent with (or slightly exceeding) the solar value, with spectral model D. This is in agreement with the results previously-reported by Buote & Fabian (1998; see also Buote 1999).

For M87, NGC 4696 and NGC 4636, we found that the fits were further significantly improved by allowing the abundances of various individual elements to be included as additional free parameters in the fits. (With spectral model D, all elements are linked to vary in the same ratio, relative to their solar values). Improvements in the measured χ^2 values of several hundred were obtained for these objects by allowing the abundances of Mg, Si and S to be included as free parameters in the fits (with only a single extra degree of freedom being associated with each extra element included as a free fit parameter). The results on the individual element abundances for M87 and NGC 4696 are discussed by Allen *et al.* (1999). The results for NGC 4636 are detailed in Section 6.

3.3 The requirement for the power-law components

The results on the power-law components detected in the ASCA spectra are summarized in Table 4. In all cases the introduction of the power-law component into the two-temperature models (models D and F) leads to a highly

Table 3. Spectral results for the central cluster galaxies

	Parameters	Model B	Model D	Model F	Model G
M87	kT	$2.02^{+0.01}_{-0.02}$	$2.19^{+0.02}_{-0.03}$	$2.17^{+0.03}_{-0.03}$	$2.01^{+0.04}_{-0.03}$
	Z_{Fe}	$0.65^{+0.02}_{-0.02}$	$0.79^{+0.04}_{-0.03}$	$0.76^{+0.04}_{-0.03}$	$0.72^{+0.04}_{-0.04}$
	N_{H}	$0.35^{+0.03}_{-0.04}$	$0.31^{+0.07}_{-0.07}$	$0.27^{+0.07}_{-0.07}$	$0.30^{+0.08}_{-0.08}$
	kT_2	—	$0.84^{+0.04}_{-0.03}$	$0.92^{+0.07}_{-0.06}$	$0.79^{+0.05}_{-0.05}$
	ΔN_{H}	—	$5.0^{+0.6}_{-0.8}$	$3.78^{+0.83}_{-1.09}$	$4.88^{+0.72}_{-0.86}$
	Γ	—	—	—	$1.40^{+0.37}_{-0.46}$
	A_1	—	—	—	137^{+159}_{-55}
	χ^2/DOF	2507/1152	1950/1149	1558/1145	1468/1143
NGC 1399	kT	$1.32^{+0.02}_{-0.03}$	$1.77^{+0.07}_{-0.07}$	—	$1.54^{+0.07}_{-0.06}$
	Z	$0.40^{+0.04}_{-0.03}$	$1.25^{+0.22}_{-0.17}$	—	$0.98^{+0.22}_{-0.15}$
	N_{H}	$0.55^{+0.11}_{-0.11}$	$0.38^{+0.25}_{-0.23}$	—	$0.44^{+0.28}_{-0.26}$
	kT_2	—	$0.78^{+0.04}_{-0.03}$	—	$0.71^{+0.04}_{-0.03}$
	ΔN_{H}	—	$2.69^{+0.79}_{-0.91}$	—	$3.57^{+0.90}_{-1.02}$
	Γ	—	—	—	$0.86^{+0.57}_{-0.63}$
	A_1	—	—	—	$5.87^{+9.73}_{-4.05}$
	χ^2/DOF	1280/792	941.8/789	—	878.6/787
NGC 4696	kT	$2.70^{+0.02}_{-0.03}$	$3.32^{+0.10}_{-0.10}$	$3.87^{+0.13}_{-0.21}$	$3.27^{+0.26}_{-0.12}$
	Z	$1.20^{+0.05}_{-0.04}$	$0.97^{+0.05}_{-0.05}$	$0.84^{+0.02}_{-0.06}$	$0.86^{+0.03}_{-0.07}$
	N_{H}	$1.09^{+0.05}_{-0.04}$	$1.44^{+0.06}_{-0.11}$	$0.89^{+0.22}_{-0.15}$	$0.96^{+0.22}_{-0.26}$
	kT_2	—	$1.40^{+0.02}_{-0.04}$	$1.52^{+0.07}_{-0.05}$	$1.46^{+0.07}_{-0.06}$
	ΔN_{H}	—	$0.00^{+0.36}_{-0.00}$	$0.71^{+0.53}_{-0.60}$	$0.59^{+1.01}_{-0.54}$
	Γ	—	—	—	$0.76^{+0.59}_{-0.65}$
	A_1	—	—	—	$22.0^{+62.1}_{-16.4}$
	χ^2/DOF	2124/755	1219/752	990.7/748	954.5/746

The best-fit parameter values and 90 per cent ($\Delta\chi^2 = 2.71$) confidence limits from the analysis of the ASCA spectra for the central cluster galaxies. Temperatures (kT), metallicities (Z), column densities (N_{H}), intrinsic column densities (ΔN_{H}), photon indices (Γ), power-law normalizations (A_1), and the normalizations of the cooler plasma emission components in spectral models D, F, G were linked to take the same values in all detectors. Only the normalizations of the hotter plasma emission components were allowed to vary independently for each detector. Temperatures are quoted in keV and metallicities as a fraction of the solar photospheric value (Anders & Grevesse 1989). Column densities and intrinsic column densities are in units of 10^{21} atom cm^{-2} . Power-law normalizations are in units of 10^{-5} photon $\text{keV}^{-1}\text{cm}^{-2}\text{s}^{-1}$ at 1 keV.

significant improvement in the fit. For guidance, a reduction in χ^2 of $\Delta\chi^2 \sim 10$ with the introduction of the power-law component (2 extra fit parameters) is significant at approximately the 99 per cent confidence level (for a fit with 1000 degrees of freedom and a reduced χ^2/DOF value ~ 1.0). The observed improvements range from $\Delta\chi^2 \sim 30$ to $\Delta\chi^2 \sim 600$.

In all cases the slopes of the power-law components are significantly flatter ($\Gamma = 0.6 - 1.5$) than the canonical value of $\Gamma \sim 1.8$ obtained for Seyfert galaxies (*e.g.* Nandra *et al.* 1997, Reynolds 1997). The weighted mean best-fit photon index for the sources in our sample is $\Gamma = 1.22$. The observed 2–10 keV fluxes range from 5.7×10^{-13} to 8.7×10^{-12} $\text{erg cm}^{-2} \text{s}^{-1}$, and the intrinsic 1–10 keV luminosities of the power-law components (corrected for Galactic and intrinsic absorption as determined with spectral model G, and calculated using the luminosity distances listed in Table 1) range from 2.6×10^{40} (NGC 4649) to 2.2×10^{42} erg s^{-1} (NGC 4696). These luminosities are also less than those typically

associated with Seyfert nuclei. Figure 1 shows the intrinsic 1–10 keV luminosities as a function of the observed photon index. No clear correlation between the two parameters is observed. Fig. 2 shows the ASCA spectrum and best-fitting model for M87 (spectral model G). For clarity, only the results for the S0 detector are shown.

The detection of hard, power-law emission components from all six galaxies is not easily explained as an artifact of the analysis. Applying the same method to an ASCA observation of NGC 1275, the dominant galaxy of the nearby ($z = 0.0183$) Perseus Cluster, which is known to contain an active nucleus, we determine a photon index for the nuclear emission of $\Gamma = 2.05 \pm 0.05$, in good agreement with the typical values determined for such galaxies (Nandra *et al.* 1997; Reynolds 1997; Turner *et al.* 1997). The 2–10 keV flux associated with the nucleus of NGC 1275, $F_{\text{X},2-10} \sim 1.8 \times 10^{-10}$ $\text{erg cm}^{-2} \text{s}^{-1}$ (implying an intrinsic 1–10 keV luminosity of $\sim 4 \times 10^{44}$ erg s^{-1}), is also significantly larger than the

Table 3. Spectral results for the Virgo ellipticals

	Parameters	Model B	Model D	Model F	Model G
NGC 4472	kT	$1.03^{+0.02}_{-0.03}$	$1.66^{+0.12}_{-0.10}$	—	$1.31^{+0.09}_{-0.06}$
	Z	$0.26^{+0.02}_{-0.02}$	$1.34^{+0.33}_{-0.24}$	—	$1.11^{+0.36}_{-0.23}$
	N_H	$0.56^{+0.15}_{-0.14}$	$0.61^{+0.56}_{-0.52}$	—	$1.65^{+0.34}_{-0.69}$
	kT_2	—	$0.77^{+0.02}_{-0.03}$	—	$0.71^{+0.03}_{-0.03}$
	ΔN_H	—	$1.10^{+1.11}_{-0.95}$	—	$0.09^{+1.12}_{-0.09}$
	Γ	—	—	—	$0.78^{+0.55}_{-0.65}$
	A_1	—	—	—	$3.82^{+5.88}_{-2.57}$
	χ^2/DOF	1006/375	536.7/372	—	474.0/370
NGC 4636	kT	$0.661^{+0.005}_{-0.006}$	$0.723^{+0.030}_{-0.021}$	$0.703^{+0.014}_{-0.014}$	$0.677^{+0.010}_{-0.009}$
	Z	$0.32^{+0.02}_{-0.02}$	$0.35^{+0.03}_{-0.02}$	$0.43^{+0.03}_{-0.04}$	$0.62^{+0.13}_{-0.09}$
	N_H	$1.42^{+0.10}_{-0.11}$	$1.50^{+0.12}_{-0.11}$	$1.24^{+0.11}_{-0.13}$	$1.03^{+0.26}_{-0.25}$
	kT_2	—	$0.550^{+0.041}_{-0.053}$	$0.509^{+0.038}_{-0.046}$	$0.387^{+0.052}_{-0.057}$
	ΔN_H	—	$0.00^{+0.03}_{-0.00}$	$0.00^{+0.23}_{-0.00}$	$2.45^{+2.00}_{-1.47}$
	Γ	—	—	—	$1.49^{+0.25}_{-0.25}$
	A_1	—	—	—	$10.4^{+4.7}_{-3.3}$
	χ^2/DOF	1512/235	1444/232	1060/229	475.0/227
NGC 4649	kT	$0.96^{+0.04}_{-0.04}$	$2.51^{+0.23}_{-0.20}$	—	$1.75^{+0.22}_{-0.26}$
	Z	$0.19^{+0.02}_{-0.03}$	$1.01^{+0.38}_{-0.28}$	—	$0.66^{+0.32}_{-0.21}$
	N_H	$0.81^{+0.30}_{-0.27}$	$0.00^{+0.13}_{-0.00}$	—	$0.00^{+0.26}_{-0.00}$
	kT_2	—	$0.79^{+0.04}_{-0.03}$	—	$0.77^{+0.05}_{-0.04}$
	ΔN_H	—	$2.11^{+0.62}_{-0.70}$	—	$2.34^{+0.66}_{-0.80}$
	Γ	—	—	—	$0.55^{+0.72}_{-0.54}$
	A_1	—	—	—	$2.24^{+5.52}_{-1.45}$
	χ^2/DOF	606.3/240	318.8/237	—	291.1/235

fluxes associated with the harder power-law components detected in the present sample of objects. Secondly, when we apply the same analysis method (using spectral model D) to an observation of the central regions of the Coma Cluster ($z = 0.0232$), where the observations are centred on the X-ray centroid of the cluster rather than an individual galaxy (the cluster does not contain a single, optically-dominant galaxy in its core), we find no improvement in the fit ($\Delta\chi^2 = 0.0$) on the introduction of a hard, power-law component. The upper (90 per cent confidence) limit to the 2 – 10 keV flux of any power-law component with a photon index $\Gamma = 2.0$ in the ASCA data for centre of the Coma Cluster using spectral model D is $F_{X,2-10} < 2.2 \times 10^{-12} \text{ erg cm}^{-2} \text{ s}^{-1}$, significantly less than the measured values for M87 and NGC 4696. We also note that the application of a similar analysis procedure to ASCA observations of more distant, luminous cooling-flow clusters does not, generally, indicate the presence of hard ($\Gamma \sim 1.2$) power-law components in these systems. (We do not expect to detect hard, power-law components with luminosities comparable to those reported here in clusters an order of magnitude (or more) more X-ray luminous than the Virgo or Centaurus clusters; *c.f.* Section 5.3) This further suggests that the hard, power-law components detected in the present sample of elliptical galaxies are not artifacts due to systematic errors

in the modeling of diffuse cluster/galaxy emission in these systems. (A more detailed discussion of the ASCA data for the Perseus and Coma clusters is presented by Allen *et al.* 1999. For a discussion of more distant, luminous cooling-flow clusters see Allen 1999).

Finally, we note that the data for NGC 4636 exhibit a systematic discrepancy at low energies ($E \lesssim 1 \text{ keV}$) between the S0 and S1 detectors, which contributes significantly to the measured χ^2 . (This discrepancy is also noted by Buote 1999). Ignoring the data in this region and repeating the analysis with spectral model G leads to a lower χ^2 value ($\chi^2 = 284$ for 201 degrees of freedom) and constraints on the power-law component in good agreement with those listed in Table 2.

3.4 A bremsstrahlung model for the hard X-ray emission

We have investigated whether the hard X-ray emission from the elliptical galaxies can also be parameterized by a simple bremsstrahlung model. To do this, the power-law component in spectral model G was replaced with a thermal bremsstrahlung component, with the temperature, kT_{brem} , and normalization, A_2 , as fit parameters. The results from the fits with this modified model are summarized in Table

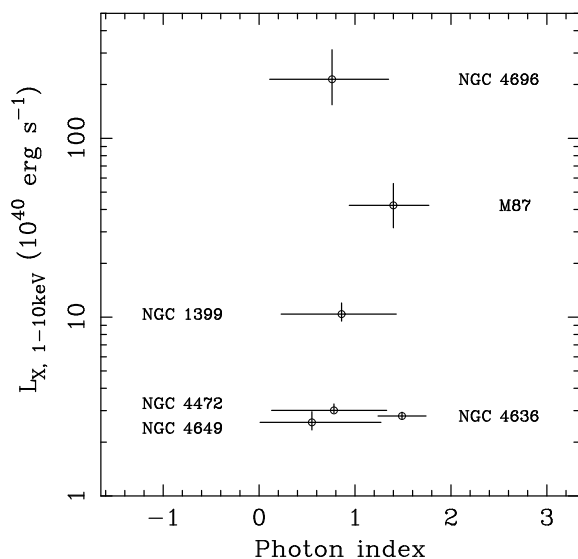


Figure 1. The intrinsic 1 – 10 keV luminosities of the detected power-law components as a function of the observed photon index, Γ . Error bars are 90 per cent ($\Delta\chi^2 = 2.71$) confidence limits. No correlation between the luminosity and photon index is observed.

5. The χ^2 values obtained indicate that the bremsstrahlung model provides as good a parameterization for the hard X-ray emission from the galaxies as the power-law model. Generally, the results constrain the temperatures of the bremsstrahlung components to be ≥ 10 keV, with the upper limits on the temperatures unconstrained. (ASCA data in the 0.6–10.0 keV band cannot reliably constrain the temperatures of plasmas hotter than ~ 10 keV). The results on the other fit parameters are essentially identical to those listed in Table 3. The fluxes and intrinsic luminosities associated with the bremsstrahlung components are also in good agreement with the values listed in Table 4, using the power-law model. The measured temperatures for the bremsstrahlung components are significantly hotter than those of typical Galactic binary sources (*e.g.* Christian & Swank 1998) and support the interpretation for the origin of the hard X-ray emission from the galaxies in terms of low radiative efficiency accretion flows, given in Section 4.

We have examined whether the statistical quality of the fits with spectral model G (or the modified model G, incorporating the bremsstrahlung component) can be improved by the addition of further model components. In all cases, the introduction of a further power-law or bremsstrahlung component did not significantly improve the fits. The introduction of a third, thermal plasma component (as described in Section 3.1) also leads to no significant improvement (at the 99 per cent confidence level) for any object, except NGC 4696. For this source, the introduction of a third plasma component (with the element abundances linked to be equal to those in the other two components) leads to a drop in χ^2 of $\Delta\chi^2 = 37$, and slightly modified constraints on the power-law emission ($\Gamma = 1.10^{+0.36}_{-0.44}$ and $A_1 = 5.8^{+6.2}_{-3.5} \times 10^{-4}$ photon $\text{keV}^{-1} \text{cm}^{-2} \text{s}^{-1}$). We note that the relatively high temperature ($kT \sim 3.3$ keV) for the hotter thermal component in

NGC 4696 simply reflects the virial temperature of the host cluster. NGC 4696 is the most distant galaxy included in the present study and the 3.7 arcmin (66 kpc) S1 aperture used includes significant flux from the extended cluster gas.

Finally, we note that several of the χ^2 values listed in Tables 3 – 5 (in particular, those for the galaxies with the highest signal-to-noise ratios in their ASCA spectra) indicate that the best-fit models are, formally, statistically unacceptable. However, the high χ^2 values obtained are primarily due to residual systematic errors in the instrument response matrices and plasma emission models (although we do not expect these to significantly effect the main conclusions reported here.)

4 THE ORIGIN OF THE HARD X-RAY EMISSION

4.1 Accretion processes

The presence of hard, power-law X-ray emission from astrophysical sources provides a discriminating signature of accretion processes around black holes. Such emission is usually attributed to the presence of a hot, tenuous coronal plasma (probably magnetically) coupled to an accretion disk or a hot (ADAF-type) accretion flow, but can also arise in the shock sites of a jet. Other astrophysical processes tend to give rise to softer X-ray emission, with a steeper photon index (when this emission is modeled as a simple power-law). The flat slopes of the power-law components detected in our sample of elliptical galaxies, together with the dynamical evidence for supermassive black holes with masses of $10^8 - 10^{10} M_\odot$ in the nuclei of these objects, argues strongly for this emission being intimately related to the accretion process.

The relatively broad point spread function of the ASCA mirrors (Section 2.2) does not allow us to resolve the X-ray emission from the galaxy cores into more than a single integrated spectrum. We therefore cannot separate the X-ray emission associated with the jets in these objects (*e.g.* knot A in M87, which previous ROSAT High Resolution Imager observations have resolved; Reynolds *et al.* 1996, Harris, Biretta & Junor 1997, 1998) from the accretion disks themselves. However, the fact that the galaxy with the strongest radio emission, M87, in which the radio and X-ray jet emission is relativistically beamed towards us, exhibits a significantly weaker hard X-ray component than NGC 4696 (which has a twin lobe radio structure and a total 4.85 GHz radio flux ~ 40 times lower than M87) at least suggests that the jet emission does not dominate the detected hard X-ray flux. This is further supported by the detections of hard, power-law X-ray components, with similar characteristic slopes, in objects such as NGC 4636, 4649, and 4472, in which the radio activity is at the level of a mJy or less. Sharp cut-offs observed in the radio spectra of these objects (Di Matteo *et al.* 1999a) also strongly constrain the populations of non-thermal particles responsible for synchrotron radiation and synchrotron self-Compton emission (in X-rays) from a jet and/or outflow associated with a low radiative-efficiency accretion flow (although contributions from a non-thermal distribution of relativistic electrons might still be important in the central cluster galaxies with more dominant radio activity; Di Matteo *et al.* 1999b).

4.1.1 The effects of intrinsic absorption

The ASCA spectra alone cannot reliably discriminate between whether the observed power-law components are intrinsically flat or have steeper photon indices which have been modified by the effects of intrinsic absorption over and above that accounted for by spectral model G. (This uncertainty is primarily due to the complex spectrum of the diffuse, thermal emission at soft X-ray energies). In general, the inclusion of an extra $\sim 5 \times 10^{22} - 10^{23}$ atom cm^{-2} of intrinsic absorption associated with the power-law components leads to power-law photon indices of $\Gamma \sim 2$, and provides similarly good fits to the ASCA data (although the determination of confidence limits on the fit parameters becomes difficult with such models). Conversely, if the true intrinsic column densities acting on the hard X-ray components are overestimated using spectral model G, then the intrinsic photon indices of these components will actually be flatter than the values listed in Table 4.

An intrinsic photon index of $\Gamma \sim 1.8 - 2$ is typically observed in AGN (*e.g.* Nandra *et al.* 1997; Reynolds 1997; Turner *et al.* 1997), where the accretion is thought to occur via a thin disk, and where the radiative efficiency is ~ 10 per cent. However, as discussed in Section 1, if the accretion in the present sample of elliptical galaxies were to proceed in this manner, the X-ray luminosities associated with their power-law emission components should be 3 – 5 orders of magnitude larger than the observed values. There is no simple way in which to modify the observed X-ray fluxes (particularly when one takes into account the joint ASCA and ROSAT results; Section 5.1) and measured photon indices to agree with the predictions from the standard thin-disk accretion models by simply including extra absorption on the power-law components.

IRAS measurements of the 60 and $100\mu\text{m}$ fluxes from the galaxies (determined using the IPAC SCANPI software applied to co-added IRAS scans) also constrain the X-ray luminosities that may be absorbed and reprocessed to infrared wavelengths in these systems. For M87, the observed 60 and $100\mu\text{m}$ luminosities ($L_{60\mu\text{m}} \sim 8 \pm 1 \times 10^{41}$ erg s^{-1} and $L_{100\mu\text{m}} \sim 4 \pm 1 \times 10^{41}$ erg s^{-1} , respectively) are comparable to the 1 – 10 keV luminosity of the hard X-ray component (Table 4). The infrared luminosities for the other galaxies are summarized in Table 6. In general, the observed $100\mu\text{m}$ luminosities do not exceed the 1 – 10 keV values by more than an order of magnitude (with the exception of NGC 4649, for which the observed $100\mu\text{m}$ luminosity is ~ 500 times larger than the 1 – 10 keV value) and the presence of an absorbed active nucleus with an X-ray luminosity 4–5 orders of magnitude more luminous in X-rays than the values listed in Table 4 can be firmly ruled out. We note, however, that although the X-ray and infrared data argue strongly against the observed hard, power-law components being due to intrinsically absorbed, steep ($\Gamma \sim 2$) X-ray spectra with luminosities $\sim 10^{46}$ erg s^{-1} , the very flat photon indices observed in some galaxies (with $\Gamma < 1$) suggest that intrinsic absorption may play some role. Such flat slopes could result from absorption of few $\times 10^{21}$ atom cm^{-2} acting on emission spectra with intrinsic photon indices, $\Gamma \sim 1.4$ (which could be produced by low-radiative efficiency accretion flows with electron temperatures $\lesssim 100\text{keV}$; Section 4.1.2). This is consistent with the observation that M87, which has an X-

ray photon index, $\Gamma = 1.4$, exhibits a lower $L_{100\mu\text{m}}/L_{\text{X},1-10}$ ratio than those galaxies with flatter X-ray slopes.

4.1.2 Low radiative efficiency accretion flows

Although the observed properties of the elliptical nuclei are not easily explained within the context of unified models for Seyfert galaxies, the characteristic hard X-ray, radio and (lack of) optical emission from these sources (*i.e.* the typically non-thermal character of their spectra) can be accounted for by models of low-radiative efficiency accretion (such as an ADAF; Narayan & Yi 1994, 1995) coupled with outflows/winds (Blandford & Begelman 1999), with the accretion occurring at approximately the Bondi rates.

In an advection dominated flow, which occurs at accretion rates $\dot{M} \lesssim \alpha^2 \dot{M}_{\text{Edd}}$ (where \dot{M}_{Edd} is the accretion rate at the Eddington limit) the viscosity (parameterized by the constant $\alpha \gtrsim 0.1$) is assumed to dissipate most of the energy locally into ions. The ions cannot cool (Coulomb scattering between the ions and electrons is very inefficient in the low density plasma; no other form of electron-ion coupling is assumed and the gas is two-temperature) and flow inwards, carrying an increasing amount of thermal energy. In the absence of an energy sink, which would normally be present in the form of efficient radiation in a thin disk, the gas will be unbound (*i.e.* have a Bernoulli parameter greater than zero) unless the binding energy is transported radially outward by the viscous torque, in the form of a wind (Blandford & Begelman 1998). Within the context of low-radiative efficiency accretion flows (unavoidably coupled with outflows), most of the accreted mass, angular momentum and energy will be lost at large distances in the flows and the central pressures and densities will be much reduced.

In these more generalized models for low-radiative efficiency accretion flows, the density varies as $\rho \propto r^{-3/2+p}$ (where the accretion rate $\dot{M} \propto r^p$, with $p \sim 1$) such that the emission in the central regions is highly suppressed. The thermal electrons, at a temperature of ~ 100 keV, radiate by synchrotron emission, inverse Compton scattering (of synchrotron photons) and bremsstrahlung emission. Most of the synchrotron emission and its Comptonization will occur in the innermost regions (within a few Schwarzschild radii) of the flow (where the temperature is the high enough, $\gtrsim 10^9$ K, for these processes to become important) and will therefore be highly suppressed in the presence of winds [†] (as emphasized by the observations and modeling discussed by Di Matteo *et al.* 1999a,b; see also Quataert & Narayan 1999). Bremsstrahlung emission, in contrast, arises from all radii in the flow and should, therefore, dominate the emission

[†] Although the luminosities due to both bremsstrahlung and synchrotron processes vary as the square of the accretion rate (*i.e.* the density), in the presence of a wind the accretion rate will be much reduced in the inner regions where most of the synchrotron emission is produced. More importantly, in the very low density inner regions the electron temperature profile is much flatter; the synchrotron power $\propto T^7$ is highly suppressed (Di Matteo *et al.* 1999b; Quataert & Narayan 1999). Comptonization of this component is also highly suppressed, its importance also depending on the scattering optical depth $\tau \propto \dot{M}$, which always remains low in the presence of a wind.

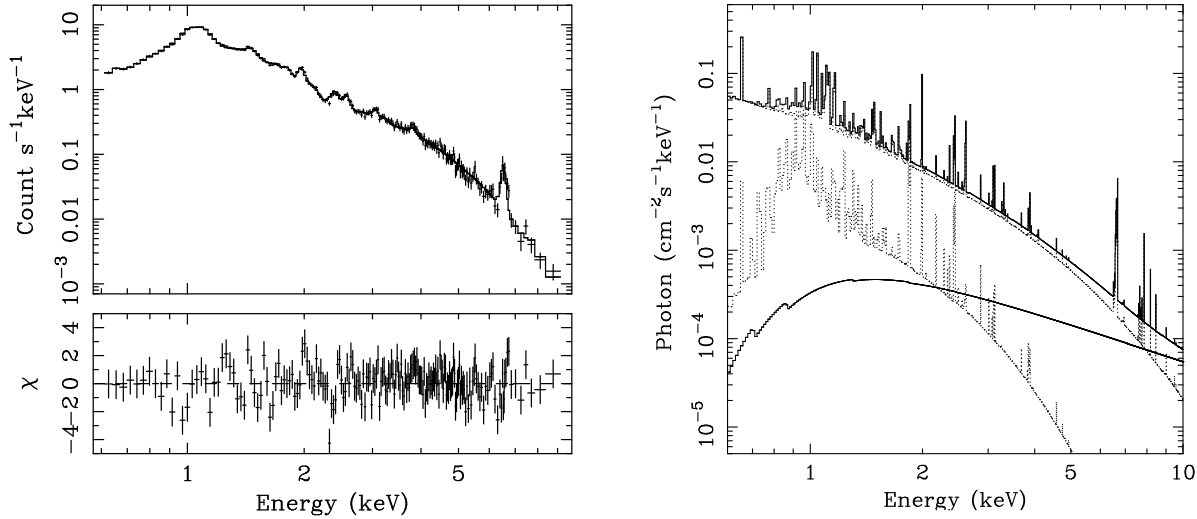


Figure 2. (Left) The ASCA S0 data and best-fitting two-temperature-plus-power-law model for M87 (with the abundances of various individual elements also included as free fit parameters; Allen *et al.* 1999) and the residuals to the fit in units of χ . (Right) The best-fit model for the S0 data, showing the relative contributions of the hot and cool plasma emission (dotted curves) and power-law components (lower solid curve) to the total flux (bold solid curve).

from sources in which low radiative efficiency accretion is associated with winds. The X-ray spectrum due to thermal bremsstrahlung in the optically thin gas has a very flat spectrum up to its cut off frequency at about $h\nu \sim kT$. Most of the bremsstrahlung luminosity, $\propto \rho^2 T^{-1/2} r^3 \exp^{-h\nu/kT}$ with $\rho \propto \alpha^{-1} M_{\text{BH}}^{-1} M r^{-3/2+p}$, originates at larger radii where the density is the highest. The temperature profile in an ADAF with winds is virtually constant with radius with $kT \approx 100 - 200 \text{ keV}$ for $r \lesssim$ a few hundred Schwarzschild radii, and tracks the virial temperature in the outer regions. Even in the presence of a very strong wind the bremsstrahlung spectrum would not be highly suppressed up to energies $kT \lesssim 10 \text{ keV}$, as the minimum temperature in the outer region of the flow is $\sim 10^{12}/r_{\text{out}} \text{ K}$ and the outer radius r_{out} is of the order of a $10^3 - 10^4$ Schwarzschild radii. As discussed by Di Matteo *et al.* (1999b), the rates at which material is required to be fed from the hot interstellar medium to the outer regions of the accretion flows, to explain the luminosities of the observed hard, X-ray components, are consistent with the expected Bondi accretion estimates of $0.1 - 1 M_{\odot} \text{ yr}^{-1}$. The emission from such a flow would be dominated by a thermal bremsstrahlung at temperatures $\lesssim 100 \text{ keV}$ (as expected in the outer regions of the flows) resembling a hard ($\Gamma \sim 1.4$) power law in the (1–10 keV) ASCA band (as required by the data). The differences in luminosity between the objects in our sample can then be ascribed to differences in the black hole masses and Bondi accretion rates, with the hard, power-law components in the central cluster galaxies being more luminous due to their higher density environments. This is illustrated in Fig. 3 where we show the intrinsic (1–10 keV) luminosities of the hard, power-law components as a function of the bolometric luminosity of the X-ray gas within a radius of 10 kpc

in the galaxies. A clear correlation between these quantities is observed, with NGC 4696, the dominant galaxy of the Centaurus Cluster and the galaxy with the most luminous hard, X-ray component, also exhibiting the largest X-ray gas luminosity within a radius of 10 kpc. Detailed modeling and discussion of these issues, and of the effects of non-thermal particle distributions in the winds and/or jets, are presented by Di Matteo *et al.* (1999b).

4.2 Other sources of X-ray emission

Although the observed properties of the hard X-ray components can be accounted for by models of low-radiative efficiency accretion onto the central supermassive black holes in the galaxies, a variety of other sources (given the large field of view of the ASCA instruments) may contribute to the integrated X-ray spectra.

4.2.1 Binary X-ray sources

Undoubtedly, some contribution towards the harder X-ray emission from the galaxies will be made by binary X-ray sources (*e.g.* Canizares, Fabbiano & Trinchieri 1987; Fabbiano 1989). Bright Galactic X-ray binaries and black-hole candidates exhibit persistent X-ray luminosities in the range $10^{36} - 10^{38} \text{ erg s}^{-1}$ (*e.g.* White *et al.* 1988). The luminosities associated with the power-law components detected in the Virgo ellipticals could therefore be accounted for by a few $10^2 - 10^4$ such sources (or $\sim 10^4 - 10^6$ sources for the more luminous central cluster galaxies). The luminosities of the power-law components in NGC 1399, 4472, 4636 and 4649 are consistent with an extrapolation of the L_X/L_B relation determined for irregular and spiral galaxies (Fabbiano

& Trinchieri 1985), in which the X-ray emission is dominated by discrete sources (binary X-ray sources, stars and central active nuclei). Thus, binary X-ray sources could contribute at a significant level (comparable to the accretion flows; see below) to the harder X-ray emission from these galaxies. For M87 and NGC 4696, however, the X-ray luminosities of the hard, power-law components are an order or magnitude larger than the values estimated from the L_X/L_B relation, based on their observed blue luminosities. Binary X-ray sources are therefore unlikely to contribute significantly to the hard, power-law components detected in M87 and NGC 4696. (The result for M87 is strongly supported by the ROSAT HRI observations discussed in Section 5.1).

In addition, although individual binary sources can exhibit very hard X-ray spectra, a more typical spectrum in the 2–10 keV band would have a photon index (using a simple power-law model) in the range $\Gamma = 1.5 - 2.5$ or, using a thermal bremsstrahlung model, a temperature, $kT \sim 4 - 7$ keV (e.g. Fabbiano *et al.* 1987; White *et al.* 1988; Makishima *et al.* 1989; Tanaka *et al.* 1996; Christian & Swank 1997), with little or no associated intrinsic absorption (Fabbiano *et al.* 1987). These power-law slopes are significantly steeper (or, equivalently, the bremsstrahlung temperatures are lower) than the observed values for the hard emission components detected in the present sample of galaxies. (We recall that the observed photon indices show no clear correlation with the luminosities of the hard, power-law components; Fig. 1). We have examined the effect of including a second power-law component, with a fixed photon index of $\Gamma = 2.0$, in the analysis of the ASCA data for NGC 4472 and 4636 with spectral model G. (We assume that the intrinsic absorption acting on both power-law components and the cooler plasma component is the same since the ASCA spectra cannot easily constrain more detailed models.) For both systems, we find that the fits are not significantly improved by the introduction of the steeper power-law components ($\Delta\chi^2 = 0.0$; see also Section 3.4), although the maximum (90 per cent confidence) 2–10 keV fluxes associated with these components (2.0×10^{-13} and 3.3×10^{-13} erg cm $^{-2}$ s $^{-1}$) are approximately 30 and 60 per cent of the values listed in Table 4, respectively. With the steeper components included at their maximum allowed levels, the photon indices of the harder power-law components in NGC 4472 and 4636 are reduced to $0.7^{+0.6}_{-1.1}$ and $0.9^{+0.3}_{-0.6}$, respectively.

We note that the relatively low source fluxes and high background count rates at harder energies, together with the broad point spread function of the ASCA mirrors, prevent us from placing useful constraints, from the ASCA imaging data, on the relative contributions to the hard X-ray fluxes from central point sources and extended emission components in the galaxies. (For M87 and NGC 4696, the extended cluster emission dominates the X-ray spectra across essentially the entire ASCA energy band; Section 5.3). Future observations with the Chandra Observatory will provide an answer to this question.

We conclude that binary X-ray sources are unlikely to dominate the hard, power-law emission detected in M87 and NGC 4696, although they will contribute to the measured fluxes in the galaxies with weaker hard, X-ray components.

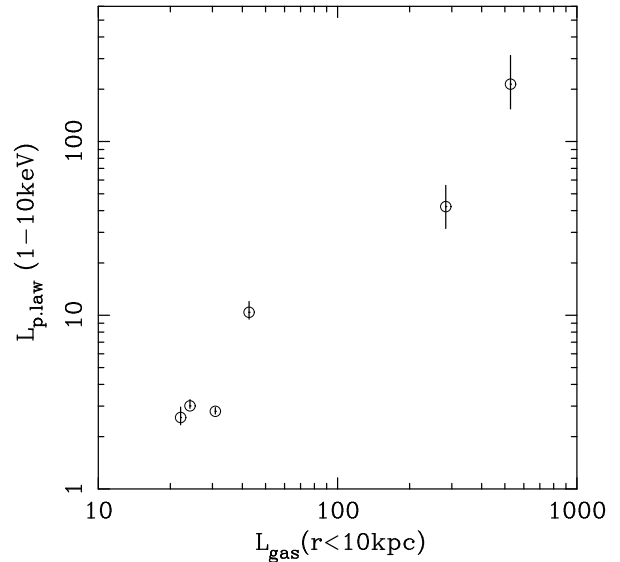


Figure 3. The intrinsic 1–10 keV luminosities of the hard, power-law components as a function of the bolometric luminosity of the X-ray gas within a radius of 10 kpc of the galaxy centres. (All luminosities are in units of 10^{40} erg s $^{-1}$.) A clear correlation between the quantities is observed, with a best-fitting slope (determined from a fit with a power-law model) of between 1 and 2.

4.2.2 Cosmic XRB fluctuations

It is important to consider the effects of fluctuations in the Cosmic XRB on the results, particularly given the close match between the weighted mean slope of the detected power-law components ($\Gamma \sim 1.2$) and the XRB ($\Gamma = 1.4$). Following Barcons, Fabian & Carrera (1998), we have estimated the confusion noise, σ_c (the flux equivalent to a $1 - \sigma$ variation in the XRB intensity histogram) for the ASCA observations. Assuming $\sigma_c = 2.0 \times 10^{-12} \Omega^{2/3}$, where Ω is the beam area of the ASCA SIS spectra in degree 2 , and normalizing to the GINGA observations of Butcher *et al.* (1997), we obtain the confusion limits listed in column 6 of Table 4. For the strongest sources (M87 and NGC 4696) the detected fluxes are much larger (a factor 40–60) than the confusion limits. For even the weakest sources (e.g. NGC 4636), the detected fluxes are 4–5 times larger than the confusion limits. We also recall that the use of an independent on-chip background-subtraction method in the analysis of the ASCA observations made in 4-CCD mode (section 2) provides very similar results on the power-law components.

4.2.3 Cosmic ray electrons and inverse Compton emission

A third mechanism that could contribute to the detected X-ray fluxes is inverse Compton emission due to primary cosmic ray electrons in the intracluster medium. Detailed models (e.g. Sarazin 1999) show that for steady particle injection (with a given power-law distribution) the inverse Compton spectra relax into a steady-state form. Although these models predict ubiquitous EUV and soft X-ray emis-

Table 4. Properties of the hard, power-law components

	FIT PARAMETERS				CON. LIMIT	STATISTICS	
	Γ	A_1	$L_{X,1-10}$	$F_{X,2-10}$	$\sigma_{c,2-10}$	$\Delta\chi^2$	χ^2/DOF
M87	$1.40^{+0.37}_{-0.46}$	137^{+159}_{-55}	$42.2^{+13.7}_{-10.6}$	$86.9^{+17.0}_{-15.6}$	1.52	90.0	1468.1/1143
NGC 1399	$0.86^{+0.57}_{-0.63}$	$5.87^{+9.73}_{-4.05}$	$10.4^{+1.6}_{-0.9}$	$9.26^{+0.30}_{-0.23}$	1.24	63.2	878.6/787
NGC 4696	$0.76^{+0.59}_{-0.65}$	$22.0^{+62.1}_{-16.4}$	214^{+99}_{-60}	$42.0^{+12.9}_{-9.9}$	1.12	38.8	954.7/746
NGC 4472	$0.78^{+0.55}_{-0.65}$	$3.82^{+5.88}_{-2.57}$	$3.01^{+0.26}_{-0.10}$	$7.09^{+0.26}_{-0.08}$	1.05	62.7	474.0/370
NGC 4636	$1.49^{+0.25}_{-0.25}$	$10.4^{+4.7}_{-3.3}$	$2.80^{+0.14}_{-0.10}$	$5.72^{+0.16}_{-0.16}$	1.32	585	475.0/227
NGC 4649	$0.55^{+0.72}_{-0.54}$	$2.24^{+5.52}_{-1.45}$	$2.58^{+0.38}_{-0.24}$	$6.21^{+0.24}_{-0.36}$	1.08	27.7	291.1/235

A summary of the results on the hard, power-law emission. Column 2 lists the measured photon indices (Γ). The normalizations of the power-law components (A_1) at an energy of 1 keV are quoted in units of 10^{-5} photon $\text{keV}^{-1}\text{cm}^{-2}\text{s}^{-1}$. Luminosities (L_X) in the 1 – 10 keV band are corrected for absorption and quoted in units of 10^{40} erg s^{-1} . The observed fluxes in the 2–10 keV band (F_X) are not corrected for absorption and are quoted in units of 10^{-13} $\text{erg cm}^{-2}\text{s}^{-1}$. σ_c values are the confusion limits for the S0 detectors in the 2 – 10 keV band in units of 10^{-13} $\text{erg cm}^{-2}\text{s}^{-1}$. The $\Delta\chi^2$ values are the improvements in χ^2 obtained with the introduction of the power-law component into the two-temperature models (either D or F as appropriate). The total χ^2 and degrees of freedom (DOF) for the fits are also listed. The errors on Γ and A_1 are the 90 per cent confidence limits ($\Delta\chi^2 = 2.71$) on a single interesting parameter. The errors on the L_X and F_X values account for the joint errors on the photon indices and normalizations.

Table 5. Additional constraints on the hard X-ray components using the bremsstrahlung model

	kT_{brem}	A_2	χ^2/DOF
M87	> 9.8	234^{+75}_{-41}	1467.1/1143
NGC 1399	> 18.0	$33.0^{+5.7}_{-6.7}$	879.5/787
NGC 4696	> 29.0	166^{+45}_{-40}	956.0/746
NGC 4472	> 18.6	$23.7^{+4.2}_{-4.4}$	475.5/370
NGC 4636	> 8.4	$14.6^{+1.8}_{-1.1}$	473.1/227
NGC 4649	> 26.0	$21.2^{+4.7}_{-8.7}$	293.3/235

A summary of the results on the hard X-ray components using the bremsstrahlung model. Column 2 lists the measured electron temperatures (kT_{brem}) in keV. Column 3 lists the normalizations (A_2) in units of 10^{-5} photon $\text{keV}^{-1}\text{cm}^{-2}\text{s}^{-1}$. Column 4 summarizes the χ^2 values (which are similar to those obtained with the power-law model in Table 4) and the numbers of degrees of freedom in the fits (DOF). Errors are 90 per cent confidence limits ($\Delta\chi^2 = 2.71$) on a single interesting parameter.

sion in clusters, due to electrons with $\gamma \sim 300$ (which have the longest loss times and could be reasonably be injected since $z \lesssim 1$), at harder energies their contribution is negligible. Significant hard X-ray emission (1 – 50 keV) can only be produced by electrons with $\gamma \sim 10^3 - 10^4$ *i.e.* by particles with rather short lifetimes (as set by inverse Compton losses; $t_{\text{loss}} \sim 10^9$ yr) and would only be present in clusters in which substantial particle injection has occurred since $z < 0.1$. Assuming that particles are accelerated in shocks in the intracluster medium, one would only expect diffuse hard X-ray emission in clusters undergoing, or having recently experienced, a major merger event. The Virgo cluster

does not show evidence for recent merger activity in its central regions (Allen *et al.* 1999). In addition, even in cases where such particle injection does occur, the expected steady state photon index where inverse Compton losses dominate would be $\Gamma \approx 2.1$, significantly steeper than the observed slopes of the power-law components.

Inverse Compton emission from the radio lobes is a further possible source of power-law X-ray emission from the galaxies. Such emission is normally very weak but has been detected from the hot-spots of Cygnus-A (Harris, Carilli & Perley 1994; Reynolds & Fabian 1996) and Fornax-A (Feigelson *et al.* 1995; Kaneda *et al.* 1995). The photon index of the resulting X-ray emission should have a photon index similar to, or steeper than, that of the radio emission which, for the radio lobes, will be significantly steeper than $\Gamma \sim 1.2$. Thus, although inverse Compton emission is expected at some level in all of the systems, it is unlikely to contribute significantly to the hard, X-ray components reported here.

4.2.4 X-ray ‘reflection’ from cold material

A final possibility for obtaining a relatively flat photon index in the ASCA band is the situation where the observed X-ray flux is dominated by photons Compton scattered off cold, optically-thick material close to the central X-ray source (*e.g.* Lightman & White 1988; George & Fabian 1991; Matt, Perola & Piro 1991). This situation also requires that the primary X-ray source is heavily obscured, a possibility argued against in Section 4.1). The scattered X-ray spectrum will include absorption and emission features due to various elements in the scattering medium and in particular should exhibit a strong, fluorescent Fe-K emission line at 6.4 keV. ASCA observations of the Circinus galaxy (Matt *et al.* 1996) and NGC 6552 (Reynolds *et al.* 1994) exhibit such ‘reflection-dominated’ spectra with strong (redshifted) 6.4 keV emission lines with equivalent widths of ~ 2 keV.

Table 6. IRAS luminosities and 6.4 keV line limits

	$L_{60\mu\text{m}}$	$L_{100\mu\text{m}}$	$L_{100\mu\text{m}}/L_{\text{X},1-10}$	E.W. _{6.4keV}
M87	78 ± 9	40 ± 10	0.95 ± 0.36	$< 90\text{eV}$
NGC 1399	< 87	81 ± 26	7.8 ± 2.7	$< 150\text{eV}$
NGC 4696	300 ± 90	900 ± 260	4.2 ± 2.1	$< 190\text{eV}$
NGC 4472	35 ± 12	21 ± 17	7.0 ± 5.7	$< 300\text{eV}$
NGC 4636	31 ± 7	< 60	< 22	$< 130\text{eV}$
NGC 4649	340 ± 10	1260 ± 20	490 ± 60	$< 210\text{eV}$

A summary of the 60 and 100 μm IRAS luminosities for the galaxies (in units of $10^{40} \text{ erg s}^{-1}$) determined with the SCANPI software and co-added IRAS scans. Error bars are the r.m.s. deviations of the residuals after baseline subtraction. Where no detection of a source was made, an upper limit equivalent to 3 times the r.m.s. deviation is quoted. Column 4 lists the ratio of the 100 μm luminosities and 1 – 10keV luminosities of the hard X-ray components. Column 5 lists the 90 per cent confidence upper limits on the equivalent widths, E.W. (in eV, relative to the power-law continua) of an intrinsic, narrow (instrumental resolution) 6.4 keV (Fe K) emission line in the ASCA spectra.

We have searched for the presence of intrinsic 6.4keV emission lines in the ASCA spectra for the galaxies. In all cases we find no improvement to the fits obtained with spectral model G on the introduction of a narrow 6.4 keV emission line ($\Delta\chi^2 = 0.0$), and are able to place 90 per cent confidence limits ($\Delta\chi^2 = 2.71$) on the maximum equivalent widths (relative to the power-law continua) of any such lines as listed in Table 6. We conclude that the flat, power-law components detected in the elliptical galaxies are unlikely to be due to this process.

4.3 Summary of the results on the origin of the hard X-ray components

We have argued that the hard ($\Gamma \sim 1.2$) power-law, X-ray components detected in the ASCA spectra are likely to be due to bremsstrahlung emission from low-radiative efficiency accretion flows onto the central supermassive black holes, coupled with winds/outflows. This is a very different situation from Seyfert galaxies, where the power-law X-ray emission is normally attributed to thermal inverse Compton scattering of the soft, disk radiation field.

We have examined a range of other mechanisms that could contribute towards the detected X-ray fluxes. Some contribution towards the harder X-ray emission could be made by the jets in these sources, although the absence of a clear correlation between the 5 GHz radio and hard X-ray luminosities suggests that the jet emission does not dominate the hard, power-law flux. The close agreement between the ASCA and ROSAT (Section 5.1) X-ray fluxes for M87, and the IRAS infrared measurements for the galaxies, argue strongly against the observed flat photon indices and low luminosities being simply due to intrinsic absorption acting on canonical Seyfert-like spectra (due to accretion at the Bondi rates with a standard radiative efficiency). Some level of intrinsic absorption is possible, however, and could explain the very flat power-law components ($\Gamma < 1$) observed in some objects (further flattening the spectra of the low-radiative efficiency accretion flows, which should have an intrinsic photon index in the ASCA band of $\Gamma \sim 1.4$). Limits on the 6.4 keV emission-line fluxes rule out a significant con-

tribution to the detected hard, power-law components from X-rays Compton scattered off cold, optically-thick matter surrounding the central X-ray sources.

Binary X-ray sources are likely to contribute to the harder X-ray emission from the galaxies with lower-luminosity power-law components (the Virgo ellipticals and NGC 1399). For M87 and NGC 4696, however, the measured power-law luminosities are an order of magnitude greater than the values predicted from the L_X/L_B relation for spiral and irregular galaxies. Moreover, the typical X-ray spectra of X-ray binaries and black hole candidates are significantly steeper than the observed hard, power-law components. Inverse Compton emission from the radio lobes in the galaxies and primary cosmic-ray electrons in the intracluster medium should not contribute significantly to the detected power-law fluxes and, where present, will typically produce a photon index in the ASCA band significantly steeper than the measured values. Fluctuations in the Cosmic XRB should not significantly effect our results.

Future X-ray observations at high spatial resolution made with the Chandra Observatory will be crucial in establishing the contributions from the various emission mechanisms outlined above and unambiguously identifying the origin of the hard X-ray components. Deep X-ray spectroscopy with XMM and ASTRO-E will allow us to examine variability in the X-ray emission and search for broad, iron emission features associated with the power-law components. If the hard X-ray emission indeed originates from bremsstrahlung processes in the outer regions of low radiative-efficiency accretion flows, then the variability timescales observed should be longer than those associated with typical Seyfert nuclei. The detection of broad iron emission features would argue against the simple, low-radiative efficiency accretion models discussed here (Section 4.1), and require the presence of significant amounts of cold, reflecting material close to the central black holes (as in standard thin-disk accretion models).

5 PREVIOUS CONSTRAINTS ON NUCLEAR X-RAY EMISSION FROM M87

5.1 ROSAT HRI observations

Reynolds *et al.* (1996) and Harris *et al.* (1997, 1998) discuss ROSAT High Resolution Imager (HRI) observations of M87, and measure a time-averaged HRI count rate associated with the active nucleus of the source of $\sim 0.12 \text{ count s}^{-1}$. We have used the XSPEC software, incorporating the 1990 December version of the HRI response matrix, to determine the flux of the power-law component required to produce the count rate observed in the $0.1 - 2.4 \text{ keV}$ ROSAT HRI band. For an assumed power-law emission model with a photon index, $\Gamma = 1.4$, absorbed by a Galactic column density, $N_{\text{H}} = 2.5 \times 10^{20} \text{ atom cm}^{-2}$, we find that a normalization, $A_1 \sim 1.5 \times 10^{-3} \text{ photon keV}^{-1} \text{ cm}^{-2} \text{ s}^{-1}$ is required to account for the observed HRI count rate. This is in excellent agreement with the value measured from the ASCA spectra of $A_1 = 1.4^{+1.6}_{-0.6} \times 10^{-3} \text{ photon keV}^{-1} \text{ cm}^{-2} \text{ s}^{-1}$. (We note that accounting for the intrinsic absorption also detected in the ASCA spectra would imply a larger intrinsic normalization for the power-law component of $A_1 \sim 5.0 \times 10^{-3} \text{ photon keV}^{-1} \text{ cm}^{-2} \text{ s}^{-1}$. However, this corrected value assumes that the absorption is due to cold gas in a uniform screen in front of the nucleus, which may not be the case *e.g.* Allen & Fabian 1997; Reynolds 1997).

5.2 Previous analyses of the ASCA observations

Two previous studies of M87 have also reported results based on the same ASCA observations discussed in this paper. Matsumoto *et al.* (1996) present results from an analysis using a simple two-temperature plasma plus power-law spectral model, with a fixed power-law photon index of $\Gamma = 1.7$, from which they determine a flux associated with the nucleus (in the $0.5 - 4.5 \text{ keV}$ band) of $1.1 \pm 0.2 \times 10^{-11} \text{ erg cm}^{-2} \text{ s}^{-1}$. This flux is ~ 2.5 times larger than the value implied by our best-fitting spectral model (model G). Reynolds *et al.* (1996) also present results from a study of the same ASCA observations, in which they did not detect significant emission associated with the nucleus, although these authors did not account for the possibility of variable element abundance ratios in their analysis, which provides a crucial step in the modeling (see also Allen *et al.* 1999). To further illustrate this, we have repeated our analysis of the power-law component in M87 with the element abundances linked to vary in the same ratio relative to their solar values (*c.f.* spectral model D). The best-fit χ^2 value obtained with this more simple model, $\chi^2 = 1888$, is substantially worse than the value, $\chi^2 = 1468$, obtained with spectral model G. The best-fit parameter values ($\Gamma = 1.70^{+0.27}_{-0.31}$ and $A_1 = 1.9^{+1.5}_{-0.9} \times 10^{-3} \text{ photon keV}^{-1} \text{ cm}^{-2} \text{ s}^{-1}$) are also (slightly) offset from the results obtained with model G. Such differences demonstrate the need to fully account for the complex temperature structure of the galaxy/cluster plasma and possible variations in individual element abundances ratios when attempting to constrain the power-law emission from such sources.

5.3 Rossi X-ray Timing Explorer observations

Reynolds *et al.* (1999) present further constraints on power-law emission from M87 using observations made with the Proportional Counter Array (PCA) on the Rossi X-ray Timing Explorer (RXTE). The data presented by these authors cover the $3 - 15 \text{ keV}$ range and constrain the $2 - 10 \text{ keV}$ flux of the power-law component to be $< 4.1 \times 10^{-12} \text{ erg cm}^{-2} \text{ s}^{-1}$, for an assumed photon index $\Gamma = 2.0$. This upper limit is lower than the measured value of $8.7^{+1.7}_{-1.6} \times 10^{-12} \text{ erg cm}^{-2} \text{ s}^{-1}$ from the ASCA data (Table 4). The ASCA data also require a significantly flatter photon index than assumed in the RXTE study.

The best-fitting spectral model for M87 determined from the ASCA analysis and plotted in Fig. 2 shows that the extended cluster emission dominates over the power-law component in the ASCA spectra across virtually the entire energy range of the detectors. Only at energies $E > 8 - 9 \text{ keV}$ does the power-law component dominate the detected flux. The much larger field of view of the PCA collimator ($\sim 1 \text{ degree}^2$ FWHM; Jahoda *et al.* 1996) results in a larger fraction of the total cluster flux (~ 5 times more) being included in the detected spectrum (the cluster emission extends to a radius of at least 4 degree ; Schindler, Binggeli & Böhringer 1999). Thus, the power-law component, as determined from the ASCA data, will not dominate over the cluster emission in the PCA spectrum below an energy of $\sim 12 - 13 \text{ keV}$.

Modelling the extended plasma emission in a cluster as cool as Virgo Cluster (Table 3) with instruments like the PCA, restricted to the (relatively hard) $3 - 15 \text{ keV}$ energy range, is difficult. The PCA spectra cannot reliably constrain the multiphase nature of the gas in the cluster core which, as this study has shown, can be crucial in constraining the properties of the power-law emission. However, although such considerations may be relevant in interpreting the RXTE results, it remains plausible that the nuclear emission from M87 may simply have varied between the ASCA observations in 1993 June and the PCA observations made in 1998 January (Harris *et al.* 1997, 1998; Tsvetanov *et al.* 1998).

5.4 ROSAT HRI flux-limits on other sources in the sample

The other galaxies discussed in this paper have not previously been studied in the same detail as M87 and no detections of point-source X-ray emission associated with their nuclei have been reported. However, Di Matteo *et al.* (1999a) present limits on possible nuclear X-ray emission for the three Virgo ellipticals, based on ROSAT HRI imaging data. Their limits, which are defined at an energy of 1 keV , are $\nu F_{\nu} < 6.8 \times 10^{-14} \text{ erg cm}^{-2} \text{ s}^{-1}$ (NGC 4472), $\nu F_{\nu} < 7.8 \times 10^{-14} \text{ erg cm}^{-2} \text{ s}^{-1}$ (NGC 4636) and $\nu F_{\nu} < 1.5 \times 10^{-13} \text{ erg cm}^{-2} \text{ s}^{-1}$ (NGC 4649). These limits compare to the measured ASCA fluxes, quoted in the same units, of $\nu F_{\nu} \sim 6.1 \times 10^{-14} \text{ erg cm}^{-2} \text{ s}^{-1}$ (NGC 4472), $\nu F_{\nu} \sim 1.6 \times 10^{-13} \text{ erg cm}^{-2} \text{ s}^{-1}$ (NGC 4636), and $\nu F_{\nu} \sim 3.5 \times 10^{-14} \text{ erg cm}^{-2} \text{ s}^{-1}$ (NGC 4649).

The ASCA measurements for NGC 4472 and 4649 are within the Di Matteo *et al.* (1999a) limits. For NGC 4636, however, the ASCA measurement is approximately twice the ROSAT limit. The Di Matteo *et al.* (1999a) limits are de-

terminated by fitting an analytic King model to the observed X-ray surface brightness profiles and determining the maximum additional contribution that can be made by a central point source. However, these limits are sensitive to complexities in the observed surface brightness profiles and, especially for NGC 4636, which exhibits a complex X-ray morphology in its central regions, the ROSAT limits should be viewed with caution.

6 THE ELEMENT ABUNDANCES IN NGC 4636

In contrast to the ASCA results for M87 and NGC 4696 (Allen *et al.* 1999), for which the introduction of individual element abundances as free parameters in the fits leads to a more significant improvement in the statistical quality of the fits than the introduction of the power-law component, for NGC 4696, the introduction of the power-law emission component provides by far the most significant improvement over the basic two-temperature model. Thus, in determining our results on the abundances of the individual elements in NGC 4636, we started from the two-temperature model with the power-law component included, which provides a χ^2 of 722.6 for 230 degrees of freedom. We then systematically determined the statistical improvements to the fit obtained by allowing the abundance of each element, in turn, to be a free parameter in the analysis. Having identified the element providing the most significant improvement, the abundance of that element was maintained as a free parameter, and the process repeated to determine the element providing the next most significant improvement.

In agreement with the results for M87 and NGC 4696, we find that the most significant improvements in the fit to the NGC 4636 data are obtained by including the abundances of Si, Mg and S as free fit parameters (the measured χ^2 value is reduced from 722.6 to 475.0, for the introduction of only three extra fit parameters). At this point, including the abundances of further elements as fit parameters did not lead to such significant improvements and, due to the already complex nature of the best-fit model, we forced the abundances of all other elements to vary with the same ratio relative to their solar values (effectively tying the abundances to that of iron, the element to which the ASCA data are most sensitive). We note, however, that including the abundances of Na and O as further free fit parameters did lead to formally significant improvements, with reductions in χ^2 of ~ 20 and 30 , respectively. However, due to the systematic uncertainties in the NGC 4636 spectra at low energies (Section 3.3), which effect the measured O abundance, and the fact that the Na abundance fits to an un-physically high value (~ 5 times solar), the metallicities of these elements were not included as free parameters in our final analysis). The measured element abundances for NGC 4636, as a fraction of their solar photospheric values defined by Anders & Grevesse (1989), are $Z_{\text{Fe}} = 0.62^{+0.13}_{-0.09}$, $Z_{\text{Mg}} = 0.93^{+0.19}_{-0.15}$, $Z_{\text{Si}} = 0.96^{+0.18}_{-0.12}$ and $Z_{\text{S}} = 1.49^{+0.27}_{-0.22}$. These results are in reasonable agreement with those of Matsushita *et al.* (1997) and Buote (1999).

Scaling our measured abundance ratios to the meteoric abundance scale of Anders & Grevesse (1989) we determine $[\text{Mg}/\text{Fe}] \sim 0.00$, $[\text{Si}/\text{Fe}] \sim 0.02$ and $[\text{S}/\text{Fe}] \sim 0.16$.

Comparing these values with the supernova yield models of Nagataki & Sato (1998), our observed $[\text{Si}/\text{Fe}]$ ratio implies a mass fraction of the iron enrichment due to type Ia supernova, $M_{\text{Fe,SNIa}}/M_{\text{Fe,total}}$, in the range $0.55 - 0.9$ (where the limits cover the full range of models examined by these authors). For spherical type II supernovae, a mass fraction in the range $M_{\text{Fe,SNIa}}/M_{\text{Fe,total}} \sim 0.7 - 0.85$ is preferred. Further comparison of our $[\text{Si}/\text{Fe}]$ constraint with the supernovae models discussed by Gibson *et al.* (1997) also requires $M_{\text{Fe,SNIa}} \sim 0.5 - 0.7$. However, the observed $[\text{S}/\text{Fe}]$ and $[\text{Mg}/\text{Fe}]$ ratios favour a mass fraction due to type Ia supernovae of $\lesssim 0.5$ (Gibson *et al.* 1997).

7 CONCLUSIONS

We have presented detections of hard X-ray emission components in the spectra of six, nearby giant elliptical galaxies observed with ASCA. The galaxies exhibit clear, dynamical evidence for supermassive ($10^8 - \text{a few } 10^9 M_{\odot}$) black holes in their nuclei. The hard X-ray emission can be parameterized by power-law models with photon indices, $\Gamma = 0.6 - 1.5$ (mean value 1.2), and luminosities, $L_{\text{X},1-10} \sim 2.6 \times 10^{40} - 2.1 \times 10^{42} \text{ erg s}^{-1}$, or thermal bremsstrahlung models with electron temperatures, $kT > 10 \text{ keV}$. Such properties identify these galaxies as a new class of accreting X-ray source, with X-ray spectra significantly harder than those of Seyfert nuclei, typical binary X-ray sources and low-luminosity AGN, and bolometric luminosities comparatively dominated by their X-ray emission. We have argued that the hard X-ray emission is likely to be due to accretion onto the central, supermassive black holes, via low-radiative efficiency flows, coupled with strong outflows. Within such models, the hard X-ray emission originates from bremsstrahlung processes in the radiatively-dominant, outer regions of the accretion flows. (Detailed modeling and discussion of these issues are presented by Di Matteo *et al.* 1999b).

For the case of M87, the flux of the hard component was shown to be in good agreement with the nuclear X-ray flux determined from earlier ROSAT HRI observations, which were able to resolve knot A in the jet from the nuclear emission component. We have stressed the importance of accounting for the complex temperature structure, intrinsic absorption and variable element abundance ratios in the analysis of the ASCA spectra. We confirmed results showing that the application of such models leads to measurements of approximately solar emission-weighted metallicities for the X-ray gas in the galaxies. We also presented detailed results on the individual element abundances in NGC 4636.

Future observations at high spatial resolution with the Chandra Observatory will be crucial in establishing the contributions from the various X-ray emission mechanisms present in elliptical galaxies and unambiguously identifying the origin of the hard X-ray components. Deep X-ray spectroscopy with XMM and ASTRO-E will allow us to examine variability in the X-ray emission (which should be slower in sources where the X-ray emission originates from the outer regions of low radiative-efficiency accretion flows than in typical Seyfert nuclei) and to search for broad, iron emission features associated with the power-law components. The detection of such broad emission features would argue

against the simple, low-radiative efficiency accretion models discussed here, and require the presence of significant amounts of cold, reflecting material close to the central black holes.

The discovery of hard X-ray emission components in the spectra of nearby elliptical galaxies containing supermassive black holes provides important new constraints on the accretion processes in these systems. Our results are relevant to understanding the demise of quasars (which could plausibly be due to a change in the dominant accretion mode in ellipticals over the history of the Universe) and, ultimately, the origin of the hard ($\Gamma \sim 1.4$) Cosmic X-ray Background (*e.g.* Di Matteo & Fabian 1997b). These issues, and others, will be explored in future papers (Di Matteo *et al.* 1999b; Di Matteo & Allen 1999).

ACKNOWLEDGEMENTS

We thank Ramesh Narayan, Eliot Quataert and Chris Reynolds for useful discussions. TDM acknowledges support for this work provided by NASA through AXAF Fellowship grant number PF8-10005 awarded by the AXAF Science Center, which is operated by the Smithsonian Astrophysical Observatory for NASA under contract NAS8-39073.

REFERENCES

- Abramowicz M.A., Chen X., Kato S., Lasota J.P., Regev O., 1995, *ApJ*, 438, L37
- Allen S.W., 1999, *MNRAS*, submitted
- Allen S.W., Fabian A.C., Johnstone R.M., Arnaud K., Nulsen P.E.J., 1999, in preparation
- Allen S.W., Fabian A.C., 1997, *MNRAS*, 286, 583
- Anders E., Grevesse N., 1989, *Geochimica et Cosmochimica Acta* 53, 197
- Arnaud K.A., 1996, in *Astronomical Data Analysis Software and Systems V*, eds. Jacoby G. and Barnes J., ASP Conf. Series volume 101, p17
- Balucinska-Church M., McCammon D., 1992, *ApJ*, 400, 699
- Barcons X., Fabian A.C., Carrera F.J., 1998, *MNRAS*, 293, 60
- Begelman M.C., Blandford R.D., Rees M.J., 1984, *Rev. Mod. Phys.*, 56, 255
- Blandford R.D., Begelman M.C., 1999, *MNRAS*, 303, L1
- Bondi H., 1952, *MNRAS*, 112, 195
- Buote D.A., 1999, *MNRAS*, preprint (astro-ph/9811080)
- Buote D.A., Fabian A.C., 1998, *MNRAS*, 296, 977
- Butcher J.A. *et al.* 1997, *MNRAS*, 291, 437
- Canizares C.R., Fabbiano G., Trinchieri G., 1987, *ApJ*, 312, 503
- Christian D.J., Swank J.H., 1997, *ApJS*, 109, 177
- Di Matteo T., Allen S.W., 1999, *MNRAS*, submitted
- Di Matteo T., Fabian A.C., 1997a, *MNRAS*, 286, L50
- Di Matteo T., Fabian A.C., 1997b, *MNRAS*, 286, 393
- Di Matteo T., Fabian A.C., Rees M.J., Carilli C.L., Ivison R.J. 1999a, *MNRAS*, 305, 492
- Di Matteo T., Quataert E., Allen S.W., Narayan R., Fabian A.C., 1999b, *MNRAS*, submitted (astro-ph/9905053)
- Fabbiano G., 1989, *ARA&A*, 27, 87
- Fabbiano G., Trinchieri G., 1985, *ApJ*, 296, 430
- Fabbiano G., Trinchieri G., van Speybroeck L.S., 1987, *ApJ*, 316, 127
- Fabian A.C., Canizares C.R., 1988, *Nature*, 333, 829
- Fabian A.C., Rees M.J., 1995, *MNRAS*, 277, L55
- Feigelson E.D., Laurent-Muehleisen S.A., Kollgaard R.I., Fomalont E.B., 1995, *ApJ*, 449, L149
- Ford H.C. *et al.* , 1995, *ApJ*, 1994, 435, L27
- George I.M., Fabian A.C., 1991, *MNRAS*, 249, 352
- Gibson B.K., Lowenstein M., Mushotzky R.F., 1997, *MNRAS*, 290, 623
- Harms R.J. *et al.* , 1994, *ApJ*, 435, L35
- Harris D.E., Biretta J.A., Junor W., 1997, *MNRAS*, 284, L21
- Harris D.E., Biretta J.A., Junor W., 1998, preprint (astro-ph/9804201)
- Harris D.E., Carilli C.L., Perley R.A., 1994, *Nature*, 367, 713
- Ho L.C., 1998, in *Observational Evidence for Black Holes in the Universe*, ed. S.K. Chakrabarti, Lumwer Academic Pub.
- Ho L.C., Filippenko A.V., Sargent W.L., 1997, *ApJ*, 487, 568
- Ishiaki *et al.* 1996, *ApJ*, 402, 441
- Kaastra J.S., Mewe R., 1993, *Legacy*, 3, HEASARC, NASA
- Kaneda H. *et al.* , 1995, *ApJ*, 453, L13
- Kormendy J., Richstone D., 1995, *ARA&A*. 33. 581
- Lightman A.P., White T.R., 1988, *ApJ*, 335, 57
- Liedhal D.A., Osterheld A.L., Goldstein W.H., 1995, *ApJ*, 438, L115
- Jahoda K., Swank J. H., Giles A. B., Stark M. J., Strohmayer T., Zhang W., Morgan E. H., 1996, in *EUV, X-ray, and Gamma-Ray Instrumentation for Astronomy VII*, ed. O. H. Siegmund, (Bellingham, WA: SPIE), 59
- Macchetto F., Marconi A., Axon D.J., Capetti A., Sparks W., Crane P., 1997, *ApJ*, 489, 579
- Magorrian J. *et al.* , 1998, *AJ*, 115, 2285
- Mahadevan R., 1997, *ApJ*, 477, 585
- Makishima *et al.* , 1989, *PASJ*, 41, 697
- Makishima *et al.* , 1994, *PASJ*, 46, L77
- Matsumoto H., Koyama K., Awaki H., Tomida H., Tsuru T., Mushotzky R., Hatsukade I., 1996, *PASJ*, 48, 201
- Matsumoto H., Koyama K., Awaki H., Tsuru T., Lowenstein M., Matsushita K., 1997, *ApJ*, 482, 133
- Matsushita K. *et al.* , 1994, *ApJ*, 436, L41
- Matsushita K., Makishima K., Rokutanda E., Yamasaki N.Y., Ohashi T., 1997, *ApJ*, 488, L125
- Matt G., Perola G.C., Piro L., 1991, *A&A*, 245, 63
- Matt G. *et al.* , 1996, *MNRAS*, 281, L69
- Nagataki S., Sato K., 1998, *ApJ*, 504, 629
- Nandra K., George I.M., Mushotzky R.F., Turner T.J., Yaqoob T., 1997, *ApJ*, 477, 602
- Narayan R., Yi I., 1994, *ApJ*, 428, L13
- Narayan R., Yi I., 1995, *ApJ*, 444, 231
- Quataert E., Narayan R., 1999, *ApJ*, submitted
- Rees M.J., Phinney E.S., Begelman M.C., Blandford R.D., 1982, *Nature*, 295, 17
- Reynolds C.S., 1997, *MNRAS*, 286, 513
- Reynolds C.S., Fabian A.C., 1996, *MNRAS*, 278, 479
- Reynolds C.S., Fabian A.C., Makishima K., Fukazawa Y., Tamura T., 1994, *MNRAS*, 268, L55
- Reynolds C.S., Di Matteo T., Fabian A.C., Hwang U., Canizares C.R., 1996, *MNRAS*, 283, L111
- Reynolds C.S., Heinz S., Fabian A.C., Begelman M.C., 1999, *ApJ*, submitted (astro-ph/9812031)
- Sadler E.M., Jenkins C.R., Kotanji C.G., 1989, *MNRAS*, 240, 591
- Sarazin C.L., 1999, *ApJ*, submitted (astro-ph/9901061)
- Schindler S., Binggeli B., Böhringer H., 1999, *A&A*, 343, 420
- Tanaka Y., 1996, *MPE Report*, 263, 85
- Tanaka Y., Inoue H., Holt S.S., 1994, *PASJ*, 46, L37
- Tsvetanov Z.I., Hartig G.F., Ford H.C., Dopita M.A., Kriss G.A., Pei Y.C., Dressel L.L., Harms R.J., 1998, *ApJ*, 493, L83
- Turner T.J., George I.M., Nandra K., Mushotzky R.F., 1997, *ApJS*, 113, 23
- White N.E., Stella L., Parmar A.N., 1988, *ApJ*, 324, 363
- Wrobel J.M., Heeshen D.S., 1991, *AJ*, 101, 148
- van der Marel R.P., 1999, *AJ*, 117, 744